Talanta 216 (2020) 120943

Contents lists available at ScienceDirect

Talanta

journal homepage: www.elsevier.com/locate/talanta

# Facile synthesis of ratiometric fluorescent carbon dots for pH visual sensing and cellular imaging

Zhonghui Guo, Yuan Jiao, Fangfang Du, Yifang Gao, Wenjing Lu, Shaomin Shuang, Chuan Dong*, Yu Wang**

*School of Chemistry and Chemical Engineering. and Institute of Environmental Science, Shanxi University, Taiyuan, 030006, PR China*

ARTICLE INFO

*Keywords:*
N
S-CDs
Ratiometric
pH visual sensing
Cellular imaging

ABSTRACT

A novel ratiometric emission N, S dual-doped carbon dots (N, S-CDs) were facilely developed for pH visual sensing via one-step hydrothermal method. The proposed N, S-CDs displayed intrinsic pH-sensitive behavior and exhibited ratiometric fluorescence emission ($F_{563\ nm}/F_{645\ nm}$) characteristic with the variation of pH values. Interestingly, a significant red shift of emission wavelength can be observed at 645 nm along with the emission at 563 nm decreased accordingly when the pH changed from 3.0 to 1.0. Simultaneously, the fluorescence of N, S-CDs aqueous solution was visually varied from yellow to red. The ratiometric pH linear response was in the region of 3.6 to 2.4 and the $pK_a$ was 2.90. Moreover, the N, S-CDs hold unique optical properties, good reversibility, superior biocompatibility and low cytotoxicity, which was further employed to monitor the intracellular pH fluctuations through the visible fluorescence changes between yellow and red. All these findings demonstrated that N, S-CDs can be utilized as the visual biosensor platform for tracking pH variations in extremely acidic environments such as gastric juice, which provided novel insights for clinical medical disease diagnosis (e.g., stomach disease detection) and other biomedical fields.

## 1. Introduction

Hydrogen ions concentration, as a significant metabolic and cellular parameter, plays a pivotal role in numerous cellular events[1], such as cellular growth and apoptosis [2], multidrug resistance [3] and other cellular processes [4,5]. Minor changes in intracellular pH may indicate abnormal cellular events and cause cell dysfunction as well as cardiopulmonary and neurological illness (e.g., cancer, Alzheimer's disease) [6–9]. Hence, the monitor of the pH in live cells is essentially significant for learning cellular function and understanding physiological and pathological process. A large amount of currently reported methods including nuclear magnetic resonance (NMR)[10], microelectrodes [11], absorption spectroscopy [12] and fluorometry[13] have been utilized for the measurement of pH values. Among them, fluorometry possesses extraordinary advantages owing to its fast response, noninvasiveness, high sensitivity and real-time monitoring [1,14]. Moreover, the fluorescent imaging offers a high spatial and temporal resolution for monitoring of pH in living cells by combined with the laser scanning confocal microscopy (LSCM) [15].

The unique structural and photophysical features of nanomaterials have opened new opportunities for fluorometry [16]. Carbon dots (CDs), as a promising candidate of nanomaterial, hold multiple advantages such as excellent optical properties, favorable biocompatibility, low toxicity and so on, which had been widely utilized as fluorescent pH nanoprobes[17–19]. These pH-sensitive CDs typically depend on single-wavelength fluorescence intensity change, which could be inevitably effected by a lot of factors including fluctuations of probe concentration, excitation source, and surrounding environment, and thus the detection accuracy may be degraded to some extent [20,21] (see Table S1). Therefore, the development of fluorescent CDs with the ratiometric characteristic enables to offer the reliability and accuracy of outcome. Ratiometric measurement with the detection of fluorescence intensities at two-well resolved wavelengths can achieve self-calibration for the environmental disturbance[14,22]. Some of the premier exploration of pH ratiometric measurements were focused on the dye-labelled CDs. Involved dyes mainly include fluorescein isothiocyanate[23,24] and rhodamine B isothiocyanate[25], which inevitably brought in other disadvantages such as complicated preparation and purification, rapid photobleaching of dyes, as well as time-consuming [20]. Therefore, great efforts have been paid to explore

* Corresponding author.
** Corresponding author.
*E-mail addresses:* dc@sxu.edu.cn (C. Dong), wangyu1168@sxu.edu.cn (Y. Wang).

https://doi.org/10.1016/j.talanta.2020.120943
Received 10 January 2020; Received in revised form 13 March 2020; Accepted 16 March 2020
Available online 20 March 2020

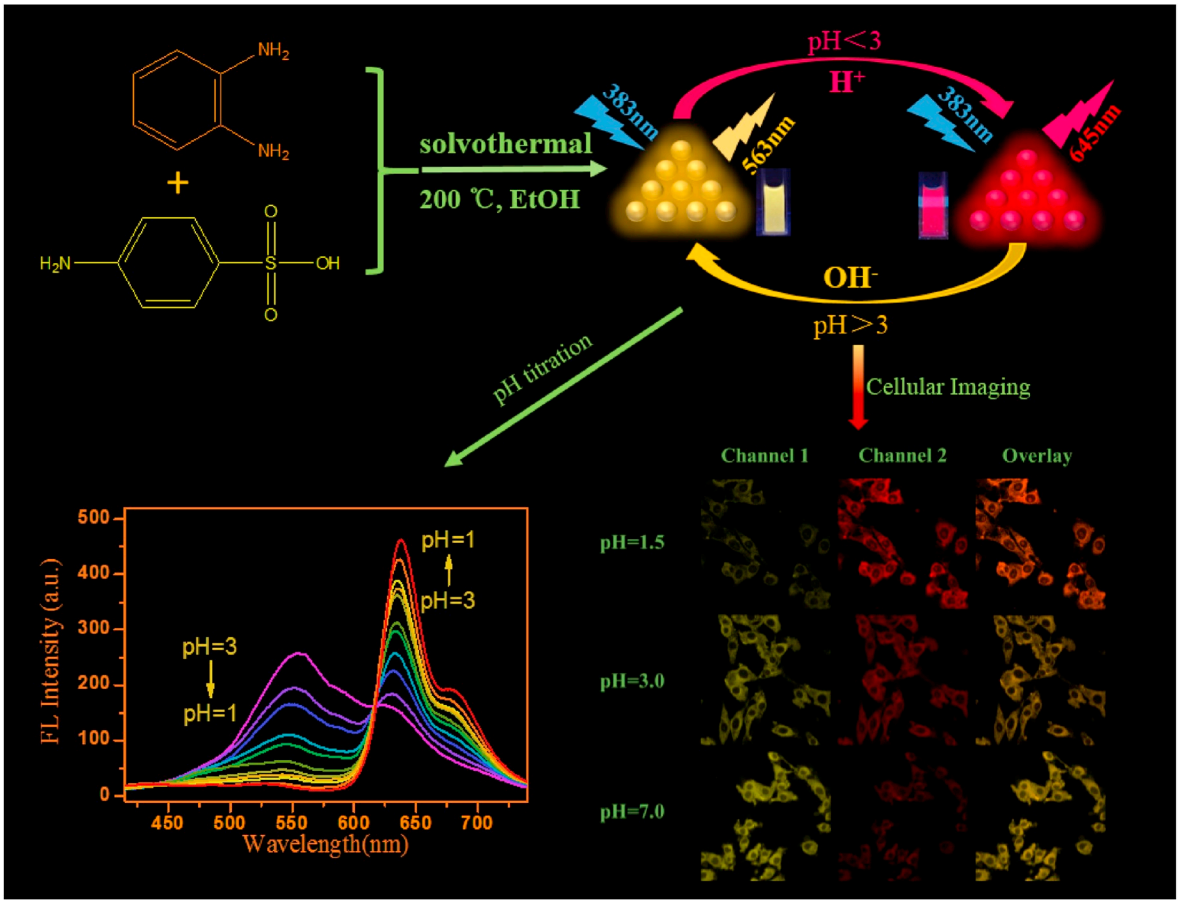


**Scheme 1.** Schematic illustration of the nanoprobe for ratiometric detection of pH and cellular imaging based on N, S-CDs.

intrinsic pH-sensitive CDs with ratiometric characteristic by facile methods rather than dye-labelling. Shang et al.[14] employed the pH-sensitive property of basic fuchsin to prepare dual emissive CDs with peaks at 475 nm and 545 nm by one-step hydrothermal method. But what is puzzling is that the emission at 545 nm matches the emission of basic fuchsin dye very well. Thus, the origin of the emission at 545 nm is still open to question. Wang and co-workers[26] further designed a N and B co-doped CDs, which endowed it ratiometric performance with two peaks at 390 and 465 nm for monitoring pH variation. Subsequently, Song[27], Xia [22] and other groups [28,29] have been developed dual-emitting CDs-based fluorescent pH nanoprobe with ratiometric features, but it was difficult to achieve the visible fluorescence variation along with significant red shift of emission wavelength. It remains a challenging issue to develop CDs with intrinsic pH-sensitive ratiometric behavior accompanied by the significant visual fluorescence changes.

Herein, we prepared a ratiometric emission N, S-CDs via one-step hydrothermal method using *o*-phenylenediamine and *p*-aminobenzenesulfonic acid as precursors (Scheme 1). The proposed N, S-CDs displayed intrinsic pH-sensitive behavior and exhibited ratiometric fluorescence emission ($F_{563\ nm}/F_{645\ nm}$) characteristic with the variation of pH values. A significant red shift of emission wavelength can be observed with the pH changed from 3.0 to 1.0, corresponding to the appearance of a new peak at 645 nm and the decrease of the emission at 563 nm accompanied by the visible fluorescence varying from yellow to red. In addition, N, S-CDs hold unique optical properties, good reversibility , rapid response time. The cytotoxicity assays also revealed that N, S-CDs possessed low toxicity and excellent cell membrane permeability, which indicated that N, S-CDs can be act as cellular markers to noninvasively monitor intracellular pH changes. The synthesized N, S-CDs were proven to be a promising nanomaterial to construct the biosensor platform for sensitive tracking pH variation, which offered novel insights for clinical medicine and other biomedical fields.

## 2. Experimental

### 2.1. Chemicals

*O*-phenylenediamine, sodium chloride (NaCl), and sodium hydroxide (NaOH), sodium dihydrogen phosphate ($NaH_2PO_4$), disodium phosphate ($Na_2HPO_4$) and absolute ethanol were obtained from Aladdin Ltd (Shanghai, China). *P*-aminobenzenesulfonic acid and concentrated phosphoric acid ($H_3PO_4$) were from Shanghai Chemical Reagent General Factory. The deionized water (18.25 MΩ·cm) was prepared through a Milli-Q Plus System (Millipore, Bedford, MA, USA) and applied in the all experiments.

### 2.2. Synthesis of the N, S-CDs

173.2 mg of *p*-aminobenzenesulfonic acid and 108.1 mg *o*-phenylenediamine were first dissolved in 20 mL of absolute ethanol, then sonicated at room temperature for half an hour. The homogeneous solution was sealed in stainless steel autoclave lined with Teflon and reacted at 200 °C for 8 h. After this, the gained dark blue suspension was centrifuged at 8000 rpm for 15 min, then filtered twice through microporous membrane (0.22 μm). The final product was collected by vacuum drying.

### 2.3. Fluorescence measurement of pH

The phosphate buffer solution (0.02 mol $L^{-1}$) with different pH values were prepared by $NaH_2PO_4$ and $Na_2HPO_4$ and titrated with

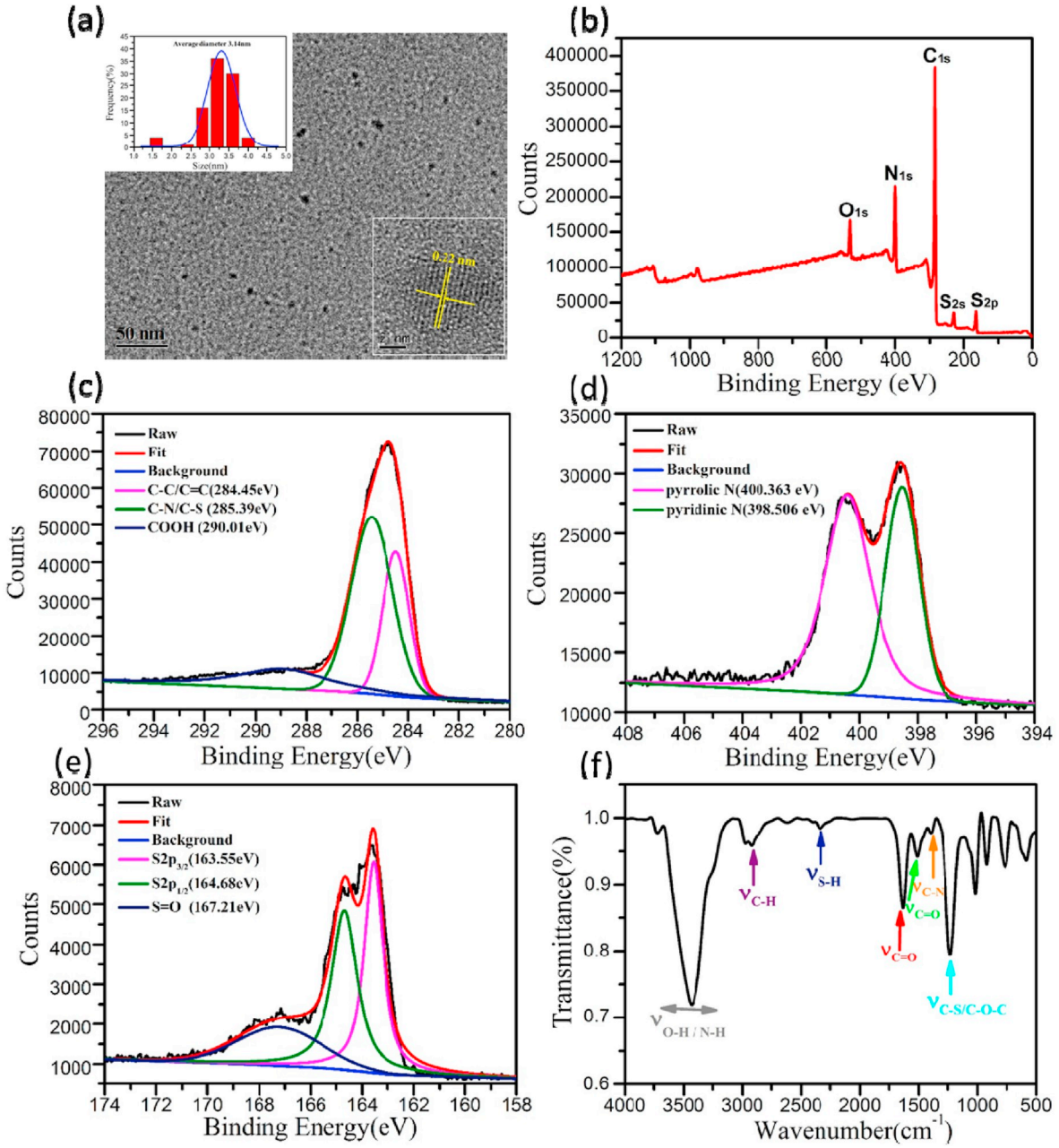


**Fig. 1.** (a) TEM, HRTEM image (inset in bottom right) and the size distribution (inset in top left) of N, S-CDs; (b) XPS survey; and the XPS high-resolution surveys of (c) $C_{1s}$, (d) $N_{1s}$ and (e) $S_{2p}$ region of N, S-CDs; (f) FTIR spectrum.

1.0 mol $L^{-1}$ $H_3PO_4$ and 1.0 mol $L^{-1}$ NaOH. In the pH titration experiment, 200 μL of N, S-CDs dispersion (8 mg $mL^{-1}$) was added into 2 mL of phosphate buffer solution with different pH values. Then the fluorescence emission spectrum were recorded with the excitation wavelength of 383 nm. All measurements were performed in triplicate at room temperature.

### 2.4. Cellular imaging

At 37 °C, SMMC7721 cells were incubated in DMEM medium containing 10% fetal bovine serum for 48 h in a 5.0% $CO_2$ atmosphere, then the medium was removed and the cells were washed three times with PBS at pH 7.4. The N, S-CDs solution (0.4 mg $mL^{-1}$) using PBS buffers of different pH as a solvent was further incubated with the cells at 37 °C for 10 min and then washed the cells again three times with PBS at pH 7.4 to remove residual N, S-CDs. The fluorescent images were collected by LSCM.

## 3. Results and discussion

### 3.1. Characterization of N, S-CDs

Transmission electron microscopy (TEM) and high resolution transmission electron microscopy (HRTEM) were chosen to investigate the particle size and morphology of the N, S-CDs. As depicted in Fig. 1a, the particles of N, S-CDs were almost spherical and monodisperse. Judging from more than 100 individual particles, the size mainly distributed between 1.4 nm and 4.2 nm with the average around 3.14 ± 0.3 nm. The inset of Fig. 1a showed the well-resolved lattice fringes spacing of 0.22 nm, which corresponded to the in-plane lattice

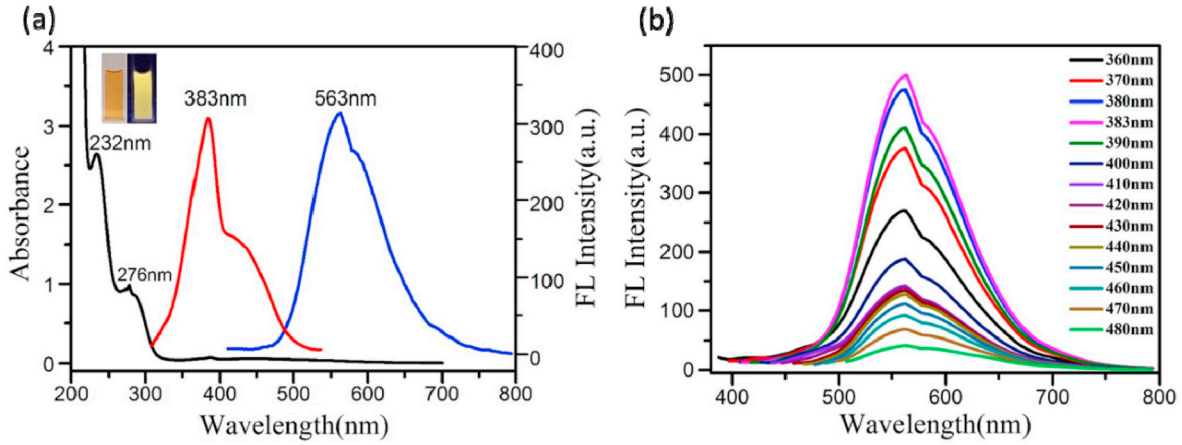


**Fig. 2.** (a) UV–vis absorption and FL spectrum of the N, S-CDs. Insert: images of N, S-CDs under sunlight (left) and UV lamp (right). (b) FL spectrum under different $\lambda_{ex}$.

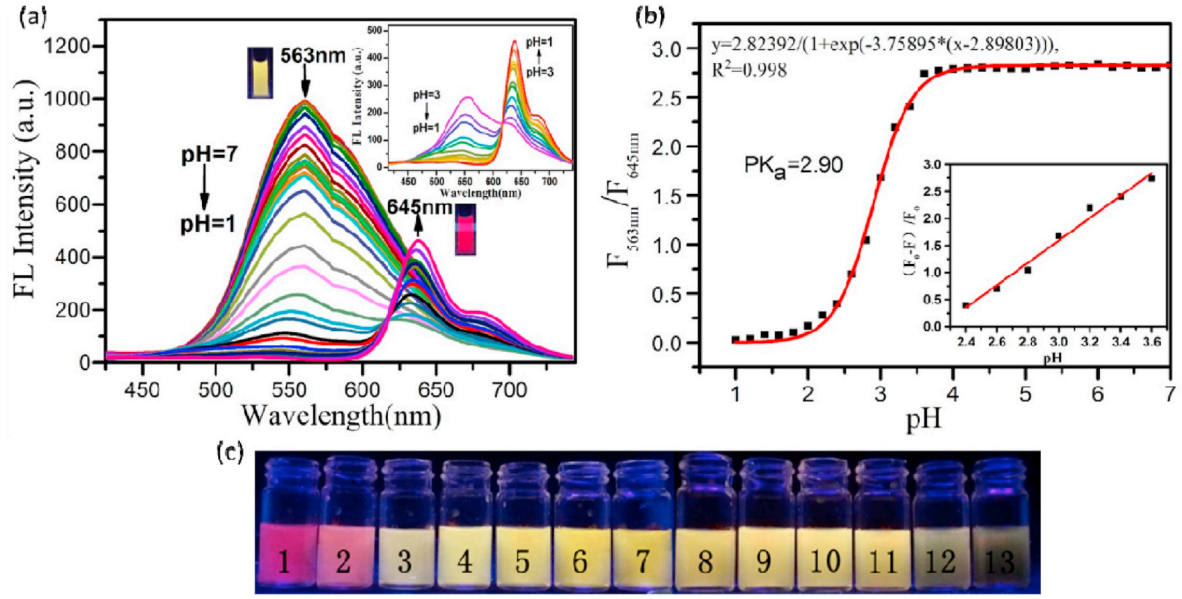


**Fig. 3.** (a) The FL spectrum of N, S-CDs (0.8 mg $mL^{-1}$) with pH values decreasing from 7.0 to 1.0, $\lambda_{ex}$ = 383 nm. (b) Sigmoidal fitting of ratiometric FL intensity ($F_{563\ nm}/F_{645\ nm}$) with different pH. The inset displayed the linear relationship of N, S-CDs against pH (2.4–3.6). (c) Picture of N, S-CDs at different pH under 365 nm UV lamp illumination.

spacing of graphite structure (100) [30]. The surface state and chemical composition of the N, S-CDs were explored via elemental analysis and X-ray photoelectron spectroscopy (XPS). As displayed in Table S2, N, S-CDs consisted of C 47.34%, H 6.05%, N 11.15%, S 11.77% and O (calculated) 23.69%, indicating that it was co-doped with S and N successfully. The XPS survey spectrum of the N, S-CDs was showed in Fig. 1b, revealing five peaks at 531.3, 398.8, 284.9, 228.9 and 163.8 eV, which should be ascribed to $O_{1s}$, $N_{1s}$, C 1s, $S_{2s}$ and $S_{2p}$, respectively[31]. The high-resolution $C_{1s}$ spectrum exhibited three main peaks at 284.5, 285.4 and 290.1 eV, which were attributed to $sp^2$ carbons (C–C/C═C), $sp^3$ carbons (C–N/C–S) and carboxyl carbons (COOH) [32], respectively (Fig. 1c). The $N_{1s}$ XPS spectrum (Fig. 1d) depicted two peaks at 398.5 and 400.3 eV, which may be caused by pyridine N and pyrrole N[33]. The $O_{1s}$ XPS spectrum (Fig. S1) could be decomposed into two peaks, which corresponded to C–O–C/C–OH (531.2 eV) and C═O (533.2 eV)[34]. The $S_{2p}$ XPS spectrum (Fig. 1e) exhibited three peaks: the peaks at 164.7 and 163.6 eV were attributed to $S_{2p\ 1/2}$ and $S_{2p\ 3/2}$ spectra of the C–S–C covalent bond[35], another higher energy peak at 167.2 eV indicated the presence of sulfate or sulfonate [36,37]. Then the functional groups of N, S-CDs were further identified by Fourier transform infrared (FTIR) spectroscopy (Fig. 1f). The absorption appeared at 3433 $cm^{-1}$ was due to the stretching vibrations of O–H and N–H. The broad peak around 2980-2920 $cm^{-1}$ were assigned to the stretching and bending vibrations of –CH, and the absorption at 2620 $cm^{-1}$ was attributed to –SH vibration [35]. In addition, the vibration peaks at 1631, 1507, 1396, 1232 and 1017 $cm^{-1}$ corresponded to C═O vibration, C═C stretching, C–NH–C stretching, C–O/C–S stretching and C–H bending, respectively [31,38]. Above analysis indicated that the results of recognition on surface functional groups by FTIR were in accordance to XPS results, and all the data manifested that the surface of N, S-CDs contained N–H, –COOH, C–N, C–S, C═O functional groups, which endowed N, S-CDs with excellent water solubility. In summary, the nitrogen and sulfur elements have been successfully incorporated into the CDs.

### 3.2. Optical properties of the N, S-CDs

The optical properties of the N, S-CDs were investigated by UV–vis absorption and fluorescence spectroscopy. The absorption spectra was depicted in Fig. 2a, the absorption peak appeared around 232 nm was

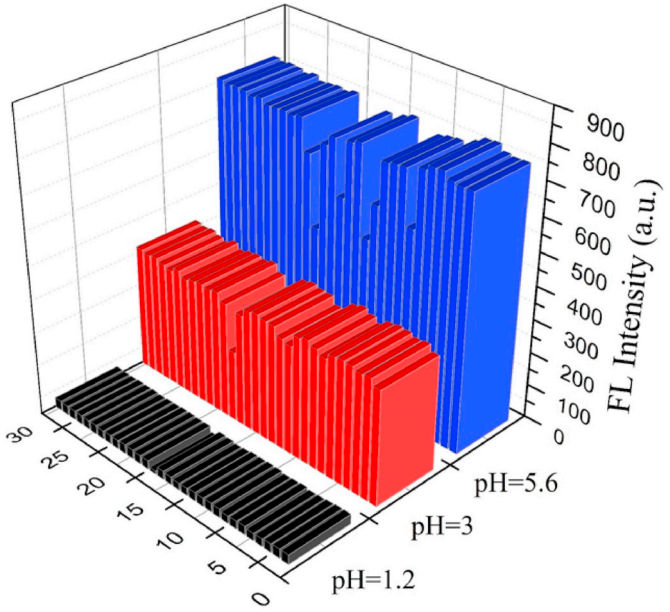


**Fig. 4.** FL intensity of N, S-CDs (0.8 mg $mL^{-1}$) in the existence of various species at pH 1.2, 3.0 and 7.0, respectively: (1) blank; (2–3) 30 mM $Na^+$, $K^+$; (4–8) 20 mM $Mg^{2+}$, $Ca^{2+}$; $Ba^{2+}$, $Zn^{2+}$; $Mn^{2+}$; (9–10) 0.1 mM $Fe^{3+}$, $Cr^{3+}$; (11–13) 1 mM $Fe^{2+}$, $Co^{2+}$, $Al^{3+}$; (14) 3 mM $Cu^{2+}$; (15) 15 mM $Ni^{2+}$; (16–17) 0.5 mM $Pb^{2+}$, $Ag^+$; (18–19) 5 mM $Cd^{2+}$, $Hg^{2+}$; (20–30) 2 mM glucose, leucine, DL-methionine, valine, L-threonine, cysteine, glycine, arginine, serine, histidine, vitamin C. ($\lambda_{ex}$ = 383 nm).

attributed to the π-π* electronic transition of the aromatic $sp^2$ domain. The absorption band at 276 nm and weak broad bands at the range of 380–630 nm were represented as the surface states, which consisted of a series of lower energy absorption bands of the functional groups[32]. Subsequently, the fluorescence behavior was performed and the result was displayed in Fig. 2a, the optical excitation and emission wavelengths of N, S-CDs were located at 383 nm and 563 nm, respectively. The inset in Fig. 2a showed the image of N, S-CDs dispersion irradiated with a 365 nm UV lamp, and it exhibited strong yellow fluorescence. Furthermore, the $\lambda_{em}$ of N, S-CDs at 563 nm was almost independent of excitation when the $\lambda_{ex}$ moved from 360 nm to 480 nm (Fig. 2b), which was attributable to the relatively uniform size distribution and surface states of the N, S-CDs. Furthermore, the quantum yield (QY) was calculated by the five-point method to be 15.97% (Fig. S2.)

The fluorescence stability of the N, S-CDs was investigated. As depicted by Fig. S3a, it was shown that even at high concentrations of NaCl (4.0 mol $L^{-1}$), the fluorescence intensity and spectral shape of N, S-CDs hardly changed, which was favorable to their practical utilization in physical salt environments. As displayed by Fig. S3b, there were no clear changes in fluorescence intensity of the N, S-CDs after continuous illumination through Xe lamp for 3 h, illustrating that N, S-CDs hold outstanding luminescence stability. Fig. S3c described the effect of different kinds of pH on N, S-CDs, the fluorescence intensity decreased significantly both in acidic and alkaline environments, implying that N, S-CDs existed great fluctuation and possessed distinct pH-sensitive feature.

### 3.3. Optical response to pH

A standard pH titration fluorescence emission spectra was conducted to study the optical response of N, S-CDs to pH. Fig. 3a showed the fluorescence spectral changes of N, S-CDs with pH, indicating the N, S-CDs possessed significant pH-dependent behavior. The emission peak at 563 nm was gradually reduced as the pH range from 7.0 to 1.0, and a new peak was proportionally emerged at 645 nm concomitantly from 3.0 to 1.0, accompanied by the fluorescence of N, S-CDs varied from yellow to red (Fig. 3c). More importantly, the apparent red shift in the fluorescence spectrum supplied a good chance to implement ratio measurement. The emission ratio ($F_{563\ nm}/F_{645\ nm}$) changed sharply from 2.83 to 0.025 in the pH range of 7.0–1.0 (Fig. 3b). According to the analysis of the emission ratio ($F_{563\ nm}/F_{645\ nm}$), sigmoidal fitting calculated $pK_a$ value of 2.90. The corresponding linear regression equation was obtained, $F_{563\ nm}/F_{645\ nm} = -4.63 + 2.07$ pH, the emission ratio also showed favorable linearity in the range of pH 3.6–2.4, and $R^2 = 0.992$. Therefore, the N, S-CDs were capable of being further applied to quantitatively determine the extreme acidic pH by conventional fluorescence and ratiometric fluorescence methods.

The recognition of N, S-CDs for $H^+$ could be attributed to the elementary morphology of nitrogen atoms on its surface. From N 1s XPS spectrum, nitrogen atoms were mainly present in the form of pyridine N and pyrrole N. The pH sensitivity was introduced via protonation or deprotonation of the pyrrole N and pyridine N moieties. The basicity of pyrrole was inferior to that of pyridine since the lone pair of electrons of pyrrole N participated in p-π conjugation[32]. Under acidic conditions, the nitrogen on the pyridine were firstly protonated, showing the gradual decrease of the fluorescence intensity at 563 nm. As the acidity was further enhanced, the pyrrole N was also protonated[39]. Simultaneously, the intramolecular charge transfer (ICT) effect between the functional groups on the surface of N, S-CDs may lead to a new peak appeared at 645 nm[1]. Moreover, the absorption spectra of N, S-CDs

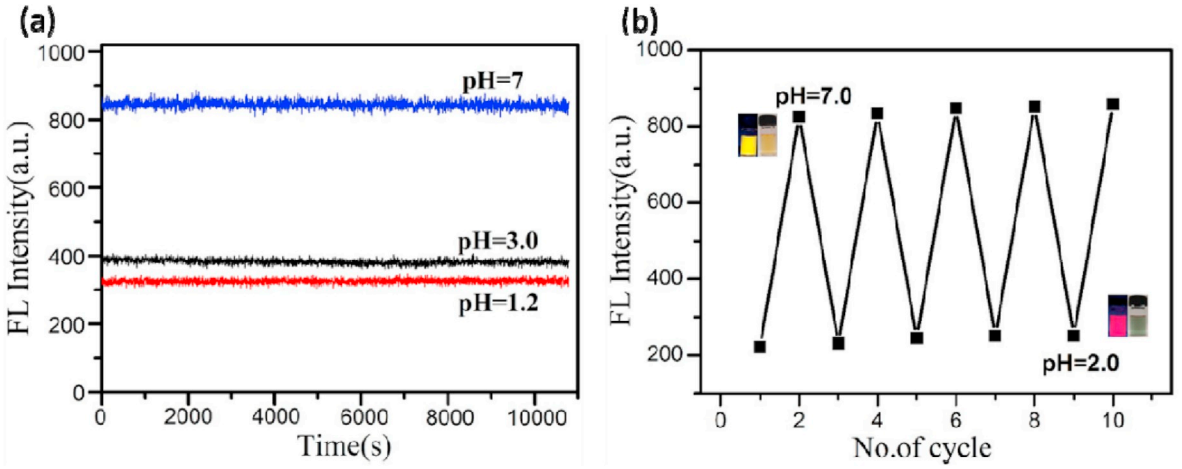


**Fig. 5.** (a) Dependence of FL intensity of N, S-CDs with time under Xe lamp irradiation at pH 7.0, 3.0 and 1.2, respectively; (b) Fluorescence reversible response against pH varied repeatedly between 7.0 and 2.0. $\lambda_{ex}/\lambda_{em}$ are 383/563 nm.

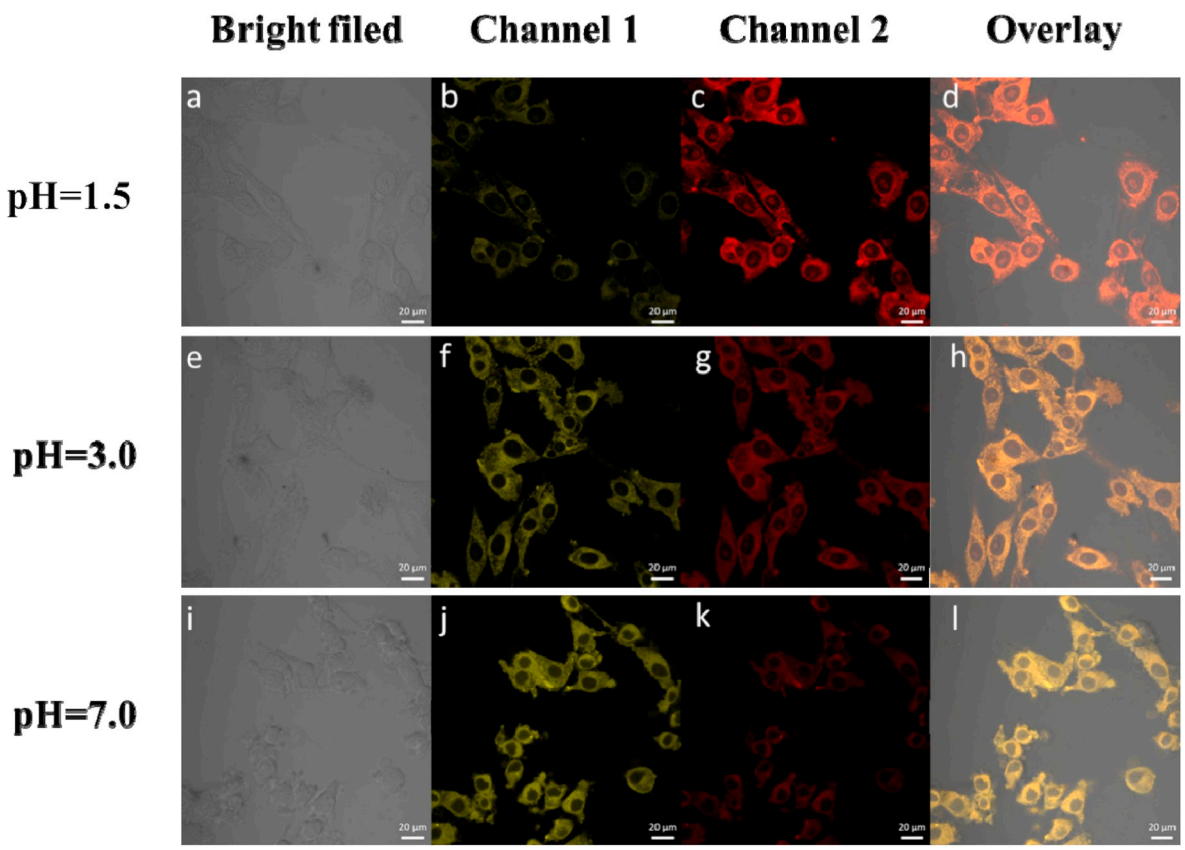


**Fig. 6.** LSCM images of N, S-CDs (0.4 mg $mL^{-1}$) in SMMC7721 cells at pH 1.5, 3.0 and 7.0, respectively. (a), (e) and (i) are the images of bright field; (b), (f) and (j) are the images of yellow channel (520–600 nm); (c), (g) and (k) are the images of red channel (600–720 nm); (d), (h) and (l) are the merged images. (For interpretation of the references to colour in this figure legend, the reader is referred to the Web version of this article.)

also showed two new bands at 574 nm and 624 nm when the pH decreased below 3.0, which corresponded to the emergence of red emission at 645 nm and 677 nm (Fig. S4). Therefore, we speculate that binding of $H^+$ to the nitrogen atoms on the N, S-CDs caused the significant fluorescence spectral response to pH. And a biosensor platform based on N, S-CDs could further established for detecting pH by this mechanism.

### 3.4. Selectivity studies

The selectivity of N, S-CDs over other metal ions and biomolecules of interest was examined at pH 1.2, 3.0 and 7.0, respectively. As demonstrated in Fig. 4, physiologically essential ions such as $Na^+$, $K^+$, $Mg^{2+}$, $Ca^{2+}$ did not cause any significant emission changes in pH measurements. Other heavy metal ions ($Fe^{3+}$, $Cu^{2+}$, $Al^{3+}$, $Hg^{2+}$, $Cr^{3+}$,$Ag^+$, $Pb^{2+}$) also exhibited no visible effects at different pH conditions. Furthermore, some bioactive molecules (e.g, glucose, leucine, DL-methionine, valine, L-threonine, cysteine, glycine, arginine, serine, histidine and vitamin C) caused negligible effects on the optical intensity of N, S-CDs. This implied that N, S-CDs exhibited high selectivity toward $H^+$, which enabled it to be a promising pH-sensitive nanoprobe for tracking $H^+$ changes.

### 3.5. Photostability and reversibility studies

Photostability is another significant factor for evaluating the capability of fluorescent CDs. The photostability of N, S-CDs at different pH (pH = 1.2, 3.0 and 7.0) was performed by recording the fluorescence intensity during 3 h ($\lambda_{ex}$ = 383 nm). As displayed in Fig. 5a, the N, S-CDs revealed excellent fluorescence stability at various pH, implying that N, S-CDs could respond immediately to changes in $H^+$ and could be utilized to observe pH changes in real time. As the reversibility is a high requirement for monitoring pH fluctuations in physiological environments. The concentrated hydrochloric acid and sodium hydroxide were used to adjust the pH value of the solution back and forth between 7.0 and 2.0 [1,29]. As depicted in Fig. 5b, neglecting the slight drift caused by instrument errors and operating errors, the results indicated that these processes were completely reversible. In a matter of seconds, the response and recovery times of the solution was fast. At the same time, the visual fluorescent colour of the solution varied between yellow (pH 7.0) and red (pH 2.0). It was obvious that N, S-CDs had a highly reversible response to pH. All the above evidences revealed that N, S-CDs possessed favorable luminescence stability and could be acted as a promising nanoprobe to monitor pH fluctuations in real time.

### 3.6. Cellular cytotoxicity assays

The cytotoxicity of N, S-CDs to living cells was assessed through standard MTT assay using SMMC7721 cells. Fig. S5 depicted the survival rate of SMMC7721 cells at different concentrations of N, S-CDs from 0 to 160 μg $mL^{-1}$. The result showed that over 81.6% of the cells were viable, indicating the N, S-CDs had low toxicity and had great potential for bioimaging of living cells in vivo.

### 3.7. Imaging of living cells

The probability of N, S-CDs for cell imaging and real-time monitoring of pH changes was explored by introducing them into SMMC7721 cells with pH 7.0, 3.0 and 1.5, respectively. Images of the second and third columns were recorded in yellow channel (520–600 nm) and red channel (600–720 nm) by 405 nm laser, respectively. As displayed in Fig. 6, N, S-CDs was well dispersed

throughout the cytoplasmic region between the nucleus and cell membrane, and exhibited a bright red fluorescence emission at pH 1.5, while yellow fluorescence was very weak (Fig. 6a–d); As the pH changed to 3.0, the red fluorescence intensity decreased and the yellow fluorescence intensity increased gradually (Fig. 6e–h); when the pH increased to 7.0, it showed a bright yellow fluorescence emission, and the red fluorescence was further lowered (Fig. 6i-l). The two channels based on the red fluorescence and yellow fluorescence displayed the characteristic pH-dependent signal, indicating that N, S-CDs possessed superior cell penetration and can be utilize in monitoring the pH variation of live cells imaging.

## 4. Conclusion

In brief, we have synthesized the ratiometric fluorescent N, S-CDs with intrinsic pH-sensitive behavior by a facile one-step hydrothermal method. The prepared N, S-CDs were implemented as a biosensor platform for pH visual sensing based on ratiometric fluorescence changes at 563 and 645 nm accompanied by the visualization fluorescence variation between yellow and red. N, S-CDs possessed excellent advantages in improving trace levels sensitivity and built-in environmental impact correction. Moreover, the N, S-CDs hold favorable photostability, superior biocompatibility, low toxicity and exceptional cell membrane permeability, which can further utilized to monitor intracellular pH in SMMC7721 cells via visible fluorescence changes between yellow and red. It is expected that the N, S-CDs could be considered as promising candidate to construct fluorescent biosensing platform for tracking pH changes in acidic environments, which provides a basis for clinical disease diagnosis and other biological fields.

## CRediT authorship contribution statement

**Zhonghui Guo:** Methodology, Software, Validation, Formal analysis, Investigation, Data curation, Writing - original draft, Writing - review & editing, Conceptualization. **Yuan Jiao:** Formal analysis, Conceptualization. **Fangfang Du:** Formal analysis. **Yifang Gao:** Formal analysis. **Wenjing Lu:** Formal analysis. **Shaomin Shuang:** Supervision, Funding acquisition, Writing - review & editing. **Chuan Dong:** Resources, Supervision, Project administration. **Yu Wang:** Supervision.

## Declaration of competing interest

The authors declare that they have no known competing financial interests or personal relationships that could have appeared to influence the work reported in this paper.

## Acknowledgements

This work was financially supported by the National Natural Science Foundation of China (No. 21874087), the Shanxi Provincial Key R&D project (201803D421031) and the Shanxi Provincial Scholarship Council of China (2017 Key1).

## Appendix A. Supplementary data

Supplementary data to this article can be found online at https://doi.org/10.1016/j.talanta.2020.120943.

## References

[1] W. Niu, L. Fan, M. Nan, Z. Li, D. Lu, M.S. Wong, S. Shuang, C. Dong, Ratiometric emission fluorescent pH probe for imaging of living cells in extreme acidity, Anal. Chem. 87 (2015) 2788.
[2] R.T. Kennedy, H. Lan, C.A. Aspinwall, Extracellular pH is required for rapid release of insulin from Zn−Insulin precipitates in β-cell secretory vesicles during exocytosis, J. Am. Chem. Soc. 118 (1996) 1795–1796.
[3] S. Simon, D. Roy, M. Schindler, Intracellular pH and the control of multidrug resistance, Proc. Natl. Acad. Sci. U.S.A. 91 (1994) 1128–1132.
[4] L. Xiao-Dong, X. Ying, S. Ru, X. Yu-Jie, L. Jian-Mei, G. Jian-Feng, A coumarin-indole-based near-infrared ratiometric pH probe for intracellular fluorescence imaging, Analyst 138 (2013) 6542–6550.
[5] R.G. Anderson, L. Orci, A view of acidic intracellular compartments, JCB (J. Cell Biol.) 106 (1988) 539–543.
[6] M. Schindler, S. Grabski, E. Hoff, S.M. Simon, Defective pH regulation of acidic compartments in human breast cancer cells (MCF-7) is normalized in adriamycin-resistant cells (MCF-7adr), Biochemistry 35 (1996) 2811–2817.
[7] A.T. Davies, E R, J.R. Johnson, A.C. Levesque, H.W. Rathbun, Non-age related differences in thrombin responses by platelets from male patients with advanced Alzheimer's disease, Biochem. Biophys. Res. Commun. 194 (1993) 537–543.
[8] I. Hiroto, T. Takayuki, I. Hiroshi, U. Hidetaka, Y. Yoichiro, T. Mizuho, I. Tomoko, M. Tadashi, Y. Takeshi, N. Minoru, Cellular pH regulators: potentially promising molecular targets for cancer chemotherapy, Canc. Treat Rev. 29 (2003) 541–549.
[9] H. Izumi, T. Torigoe, H. Ishiguchi, H. Uramoto, Y. Yoshida, M. Tanabe, T. Ise, T. Murakami, T. Yoshida, M. Nomoto, Cellular pH regulators: potentially promising molecular targets for cancer chemotherapy, Canc. Treat Rev. 29 (2003) 541–549.
[10] H. Sja, G.D.C. Ruijter, J. Visser, Measurement of intracellular (compartmental) pH by P-31 NMR in aspergillusniger, J. Biotechnol. 77 (2000) 5–15.
[11] D. Ellis, R.C. Thomas, Microelectrode measurement of the intracellular pH of mammalian heart cells, Nature 262 (1976) 224.
[12] J. Han, K. Burgess, Fluorescent indicators for intracellular pH, Chem. Rev. 110 (2010) 2709–2728.
[13] H. Szmacinski, J.R. Lakowicz, Optical measurements of pH using fluorescence lifetimes and phase-modulation fluorometry, Anal. Chem. 65 (1993) 1668–1674.
[14] J. Shangguan, D. He, X. He, K. Wang, F. Xu, J. Liu, J. Tang, X. Yang, J. Huang, Label-Free carbon-dots-based ratiometric fluorescence pH nanoprobes for intracellular pH sensing, Anal. Chem. 88 (2016) 7837–7843.
[15] F. Li, Q. Liu, D. Lu, H. Shi, Y. Yang, Y. Li, C. Dong, S. Shuang, A novel far-visible and near-infrared pH probe for monitoring near-neutral physiological pH changes: imaging in live cells, J. Math. Chem. B 1 (2013) 4281–4288.
[16] G.M. Zhang, T. Xu, H.Z. Du, Y.Y. Qiao, X.H. Guo, L.H. Shi, Y. Zhang, S.M. Shuang, C. Dong, H.M. Ma, A reversible fluorescent pH-sensing system based on the one-pot synthesis of natural silk fibroin-capped copper nanoclusters, J. Mater. Chem. C 4 (2016) 3540–3545.
[17] X. Jin, X. Sun, G. Chen, L. Ding, Y. Li, Z. Liu, Z. Wang, W. Pan, C. Hu, J. Wang, pH-sensitive carbon dots for the visualization of regulation of intracellular pH inside living pathogenic fungal cells, Carbon 81 (2015) 388–395.
[18] J. Xiaofang, L. Jing, W. Erkang, One-pot green synthesis of optically pH-sensitive carbon dots with upconversion luminescence, Nanoscale 4 (2012) 5572–5575.
[19] W. Kong, H. Wu, Z. Ye, R. Li, T. Xu, B. Zhang, Optical properties of pH-sensitive carbon-dots with different modifications, J. Lumin. 148 (2014) 238–242.
[20] Q. Songnan, C. Hong, Z. Xuanming, C. Junsheng, L. Xingyuan, Ratiometric fluorescent nanosensor based on water soluble carbon nanodots with multiple sensing capacities, Nanoscale 5 (2013) 5514–5518.
[21] Y.H. Yan, J. Sun, K. Zhang, H.J. Zhu, H. Yu, M.T. Sun, D.J. Huang, S.H. Wang, Visualizing gaseous nitrogen dioxide by ratiometric fluorescence of carbon nanodots-quantum dots hybrid, Anal. Chem. 87 (2015) 2087–2093.
[22] C. Xia, M. Cao, F.J. Xia, G. Zhou, H. Li, An ultrafast response and sensitive ratiometric fluorescence pH nanoprobe based on label-free dual-emission carbon dots, J. Mater. Chem. C (2019) 7.
[23] X. Zhu, H. Jin, C. Gao, R. Gui, Z. Wang, Ratiometric, visual, dual-signal fluorescent sensing and imaging of pH/copper ions in real samples based on carbon dots-fluorescein isothiocyanate composites, Talanta 162 (2017) 65–71.
[24] W. Liu, C. Li, X. Sun, P. Wei, J. Wang, Carbon-dot-based ratiometric fluorescent pH sensor for the detections of very weak acids assisted by auxiliary reagents that contribute to the release of protons, Sensor. Actuator. B Chem. 244 (2017) 441–449.
[25] W. Shi, X. Li, H. Ma, A tunable ratiometric pH sensor based on carbon nanodots for the quantitative measurement of the intracellular pH of whole cells, Angew. Chem. 51 (2012) 6432–6435.
[26] Y. Wang, L. Lu, H. Peng, J. Xu, F. Wang, R. Qi, Z. Xu, W. Zhang, Multi-doped carbon dots with ratiometric pH sensing properties for monitoring enzyme catalytic reactions, Chem. Commun. 52 (2016) 10.1039.C1036CC02874H.
[27] W. Song, W. Duan, Y. Liu, Z. Ye, Y. Chen, H. Chen, S. Qi, J. Wu, D. Liu, L. Xiao, Ratiometric detection of intracellular lysine and pH with one-pot synthesized dual emissive carbon dots, Anal. Chem. 89 (2017) 13626–13633.
[28] A. Chandra, N. Singh, Biocompatible fluorescent carbon dots for ratiometric intracellular pH sensing[J], Chemistry 2 (20) (2017) 5723–5728.
[29] H. Nie, M.J. Li, Q.S. Li, et al., Carbon dots with continuously tunable full-color emission and their application in ratiometric pH sensing[J], Chem. Mater. 26 (10) (2014) 3104–3112.
[30] J. Zhan, B.J. Geng, K. Wu, et al., A solvent-engineered molecule fusion strategy for rational synthesis of carbon quantum dots with multicolor bandgap fluorescence[J], Carbon 130 (2018) 153–163.
[31] M.R. Zhang, R.G. Su, J. Zhong, L. Fei, W. Cai, Q.W. Guan, W.J. Li, N. Li, Y.S. Chen, L.L. Cai, Q. Xu, Red/orange dual-emissive carbon dots for pH sensing and cell imaging, Nano Research 12 (2019) 815–821.
[32] J. Yuan, G. Xiaojuan, h. Hui, G. Yifang, L. Wenjing, l. Yang, X. Ming, S. Shaomin, D. Chuan, Facile synthesis of orange fluorescence carbon dots with excitation independent emission for pH sensing and cellular imaging, Anal. Chim. Acta 1042 (2018) 125–132.
[33] Y.Y. Ding, X.J. Gong, Y. Liu, W.J. Lu, Y.F. Gao, M. Xian, S.M. Shuang, C. Dong, Facile preparation of bright orange fluorescent carbon dots and the constructed biosensing platform for the detection of pH in living cells, Talanta 189 (2018) 8–15.

[34] X. Gong, W. Lu, C.P. Man, Q. Hu, X. Wu, S. Shuang, C. Dong, M.M.F. Choi, Facile synthesis of nitrogen-doped carbon dots for Fe 3+ sensing and cellular imaging, Anal. Chim. Acta 861 (2015) 74–84.

[35] H. Shan, Y. Erli, Y. Jiandong, L. Yi, X. Qi, Red emission nitrogen, boron, sulfur co-doped carbon dots for “on-off-on” fluorescent mode detection of Ag + ions and l -cysteine in complex biological fluids and living cells, Anal. Chim. Acta 1035 (2018) 192–202.

[36] S.M. Song, F. Liang, M.L. Li, F.F. Du, W.J. Dong, X.J. Gong, S.M. Shuang, C. Dong, A label-free nano-probe for sequential and quantitative determination of Cr(VI) and ascorbic acid in real samples based on S and N dual-doped carbon dots, Spectrochim. Acta Mol. Biomol. Spectrosc. 215 (2019) 58–68.

[37] H.Y. Wang, Q.J. Lu, Y.X. Hou, Y.L. Liu, Y.Y. Zhang, High fluorescence S, N co-doped carbon dots as an ultra-sensitive fluorescent probe for the determination of uric acid, Talanta 155 (2016) 62–69.

[38] X. Gong, H. Wang, Y. Liu, Q. Hu, Y. Gao, Z. Yang, S. Shuang, C. Dong, A di-functional and label-free carbon-based chem-nanosensor for real-time monitoring of pH fluctuation and quantitative determining of Curcumin, Anal. Chim. Acta 1057 (2019) 132–144.

[39] W. Lu, Y. Jiao, Y. Gao, J. Qiao, M. Mozneb, S. Shuang, C. Dong, C.-Z. Li, Bright yellow fluorescent carbon dots as a multi-functional sensing platform for the label-free detection of fluoroquinolones and histidine, ACS Appl. Mater. Interfaces 10 (2018) 42915–42924.